Supplemental Material: "Observation of a Strong Atom-Dimer Attraction in a Mass-Imbalanced Fermi-Fermi Mixture"

Michael Jag[1,2], Matteo Zaccanti[1,3], Marko Cetina[1], Rianne S. Lous[1,2], Florian Schreck[1], and Rudolf Grimm[1,2]
[1] *Institut für Quantenoptik und Quanteninformation (IQOQI), Österreichische Akademie der Wissenschaften*
[2] *Institut für Experimentalphysik, Universität Innsbruck, 6020 Innsbruck, Austria and*
[3] *CNR Istituto Nazionale Ottica, 50019 Sesto Fiorentino, Italy*

Dmitry S. Petrov[1] and Jesper Levinsen[2,3]
[1] *Université Paris-Sud, CNRS, LPTMS, UMR8626, Orsay, F-91405, France*
[2] *TCM group, Cavendish Laboratory, JJ Thomson Avenue, Cambridge, CB3 0HE, United Kingdom and*
[3] *Aarhus Institute of Advanced Studies, Aarhus University, DK-8000 Aarhus C, Denmark*
(Dated: November 20, 2013)

A. Light shift of the Feshbach resonance

The Feshbach resonance (FR) that we employ for tuning the interactions in our system occurs between ^{6}Li atoms in their lowest internal state, denoted Li$|1\rangle$ ($f = 1/2, m_f = +1/2$), and ^{40}K atoms in their third-to-lowest state K$|3\rangle$ ($f = 9/2, m_f = -5/2$). This resonance has been investigated in detail in Ref. [1]. The magnetic field dependent Li-K s-wave scattering length is given by

$$a(B) = a_{\rm bg}\left(1 - \frac{\Delta}{B - B_0}\right) \qquad (1)$$

where $a_{\rm bg} = 63.0\,a_0$ is the background scattering length, $\Delta = 0.88\,$G is the width, and B_0 is the center of the resonance near 154.7 G.

As we already pointed out in Ref. [2], the optical trap induces a differential light shift between the atom pair state and the molecular state. This leads to a light-induced shift of the FR center. For the experiments presented in the main text, we use a near-infrared laser with a wavelength of 1064 nm (single-mode operation) in three different trap settings. Therefore, the center of the FR needs to be determined for each trap setting.

To determine B_0 we perform radio-frequency (rf) spectroscopy of the Feshbach molecules. For each trap setting, this is done in the following way: We prepare a nonresonant mixture of Li atoms in state Li$|1\rangle$ and K atoms in their second-to-lowest state K$|2\rangle$ several tens of mG below the approximate position of the resonance center. Here, we apply a strong 500-μs rf pulse at a variable frequency ν, several kHz below the unperturbed K$|2\rangle\rightarrow$K$|3\rangle$ transition frequency ν_0. This pulse drives Li$|1\rangle$-K$|2\rangle$ atom pairs into the Li$|1\rangle$K$|3\rangle$ dimer state. To determine the number of dimers associated, we subsequently dissociate the dimers into a Li$|1\rangle$ and a K$|3\rangle$ atom by a 300-μs magnetic field ramp to 154.8 G. By recording absorption images we then determine the populations N_2 and N_3 of the K spin states K$|2\rangle$ and K$|3\rangle$, respectively.

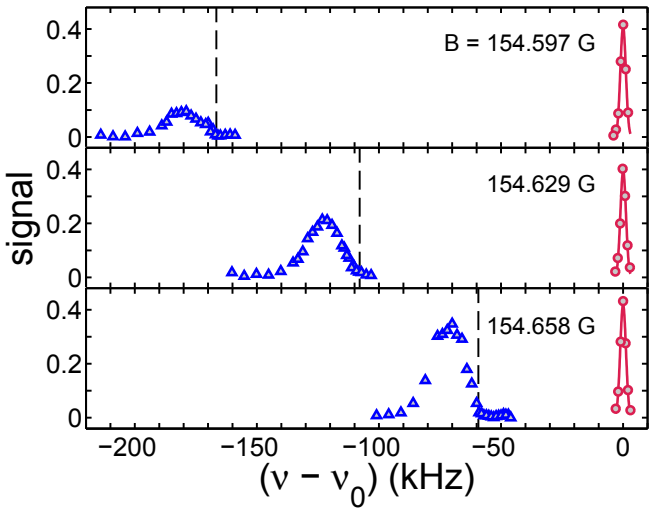

FIG. 1: Data from the molecular rf association spectroscopy in trap 2. Red circles were taken with a rf power set to the value to match the π-pulse condition in the absence of interactions (no Li$|1\rangle$ present) and is scaled by 0.5. Blue points were taken with a 30× larger rf power. The dashed lines indicate the binding energy $E_{\rm b}(B)$.

By plotting the signal, given by $N_3/(N_3+N_2)$, against the rf detuning $\nu - \nu_0$, we resolve the molecule association spectrum; see Fig. 1. The unperturbed transition frequency ν_0, corresponding to the Zeeman splitting of the two states, is determined by rf spectroscopy in the absence of Li$|1\rangle$ (red points). We determine the binding energy of the molecules from the onset frequency of the molecular association spectra. As the onset frequency, we use the upper rf frequency at which the fraction of atoms transferred is roughly 10% of its peak height. We have checked that, within the errors of our measurements, this criterion agrees with the result obtained by fitting the line-shape model [3] to the spectra, as was done in Ref. [2]. This procedure is repeated for each trap power at various magnetic fields.

We then fit a model [2] for the molecular binding energy near our FR to the data with B_0 as the only free

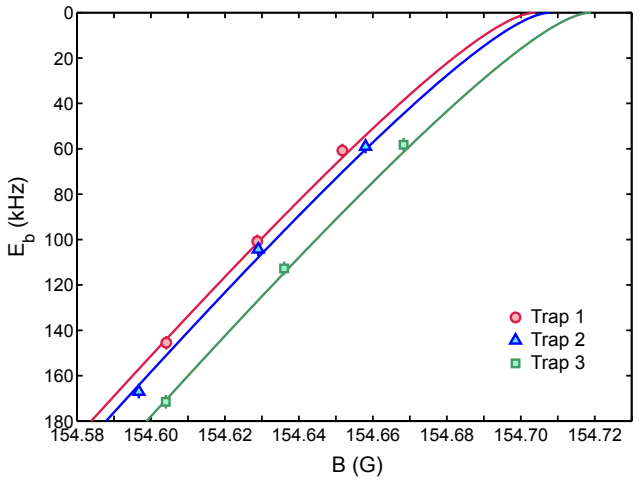

FIG. 2: Determination of the FR center B_0 by rf association of dimers. The points show the experimentally determined molecular binding energies $E_\mathrm{b}(B)$ for the three trap settings. The solid curves are fits of a theoretical model (see text) to the experimental data.

parameter; see Fig. 2. This procedure allows us to determine the resonance center in each trap setting with an uncertainty of ± 2 mG. The accuracy of our determination of the resonance position is limited by the uncertainty in the FR parameters [1] used in the model for the binding energy. We determine the center of the FR of trap 1, 2, and 3 to be at the magnetic field of 154.704 G, 154.708 G, and 154.719 G, respectively.

B. Preparation of the atom-dimer mixture

To cool our atomic sample, we evaporate a Li$|1\rangle$-Li$|2\rangle$ spin mixture at a magnetic field near 1150 G on the attractive side of the 834-G Li$|1\rangle$-Li$|2\rangle$ Feshbach resonance in a single-beam optical dipole trap [4]. During evaporation, a few 10^4 K atoms are sympathetically cooled by the Li environment. The endpoint of evaporation is always set to the same final value. After evaporation, we follow the scheme described in Ref. [4] to transfer the atoms into a crossed-beam optical dipole trap and reach a magnetic field of 154.8 G with typically 10^6 Li atoms in state Li$|1\rangle$ and 4×10^4 K atoms in state K$|1\rangle$. We finally vary the temperature of our sample by increasing the power of our crossed beams to adiabatically recompress the trapped sample. This scheme allows us to maintain a similar population imbalance and degeneracy for the three trap settings used.

To prepare for dimer association, we first create a weakly interacting Li$|1\rangle$-K$|3\rangle$ mixture at B_0+180 mG. A first rf pulse transfers ~80% of the K$|1\rangle$ population into state K$|2\rangle$ and a second rf pulse then transfers the total K$|2\rangle$ population into the interacting state K$|3\rangle$. The ~7 000 K atoms, which remain in the K$|1\rangle$ state, later serve for the spectroscopy.

We associate dimers using a two-step magnetic field ramp. In a first 20-ms step we ramp the magnetic field from B_0+180 mG to B_0+5 mG. This ramp is sufficiently slow for the Li atoms to be attracted into the regions of high K density, increasing the density overlap between the two clouds. We then associate the Li$|1\rangle$K$|3\rangle$ dimers via a 0.5-ms Feshbach ramp to B_0-17 mG. We note that, during these magnetic field ramps, two-body inelastic losses [1] are negligible.

To obtain a pure sample of about 15 000 Li$|1\rangle$K$|3\rangle$ dimers, we remove all unbound atoms from the states Li$|1\rangle$ and K$|3\rangle$. The Li$|1\rangle$ atoms are removed by a sequence of rf and laser pulses. This procedure consists of a first 250-μs rf pulse resonant with the free Li$|1\rangle\rightarrow$Li$|2\rangle$ transition, followed by a 10-μs resonant light pulse, which selectively removes the Li$|2\rangle$ atoms from the trap. This scheme removes about 95% of the excess Li atoms without causing any observable loss of KLi dimers. A second 250-μs rf pulse transfers the leftover 5% of Li$|1\rangle$ atoms into the noninteracting Li$|2\rangle$ state, where they remain without further affecting the experiment.

Simultaneously with this "double-cleaning" of the unbound Li atoms, we remove the unbound K$|3\rangle$ atoms in a similar way. Using a 90-μs rf pulse resonant with the K$|3\rangle\rightarrow$K$|2\rangle$ transition, followed by a second 145-μs rf pulse resonant with the K$|3\rangle\rightarrow$K$|4\rangle$ transition, we empty the K$|3\rangle$ state with >99 % efficiency. The pulse lengths are chosen such that they are short, i.e. spectroscopically wide, compared to the frequency shifts due to atom-dimer and atom-atom interactions but long, i.e spectroscopically narrow, compared to the binding energy $E_\mathrm{b} = h\times 17$ kHz (h is Planck's constant) of the dimers, avoiding the dissociation of dimers.

In a final step, the ~7 000 K atoms which resided in state K$|1\rangle$ during the entire dimer association process, are transferred in the K$|2\rangle$ state and thus prepared for the rf spectroscopy. This is accomplished by a rf pulse which flips the K$|1\rangle$ and K$|2\rangle$ populations. We note that these K atoms remain unaffected by the dimer association since their interactions with the other components are negligible over the timescales of the experiment.

From here, we reach the specific magnetic field detunings $B-B_0$, at which the spectroscopy is performed, by a 200-μs magnetic field ramp.

C. Determination of the temperatures and the densities

Here, we describe how we determine the temperatures and the densities of the atom cloud and the dimer cloud. The resulting experimental parameters are summarized in Table I.

Atom and dimer temperatures – The temperatures of our atom and dimer clouds are obtained by Gaussian fits to absorption images of the clouds after a long time-of-flight of $t_\mathrm{tof}=6$ ms. With the measured radial Gaussian

Trap	$T_{\rm eff}$ (nK)	$T_{\rm K}$ (nK)	$\bar{T}_{\rm D}$ (nK)	$\nu_{r,{\rm K}}$ (Hz)	$\nu_{a,{\rm K}}$ (Hz)	$\nu_{r,{\rm Li}}$ (Hz)	$\nu_{a,{\rm Li}}$ (Hz)	$\nu_{r,{\rm D}}$ (Hz)	$\nu_{a,{\rm D}}$ (Hz)	$\sigma_{r,{\rm K}}$ (μm)	$\sigma_{a,{\rm K}}$ (μm)	$\bar{\sigma}_{r,{\rm D}}$ (μm)	$\sigma_{a,{\rm D}}$ (μm)
1	165(15)	138(5)	195(15)	197(5)	25.5(10)	314(5)	34.0(10)	216(5)	27.0(10)	4.3(1)	33(2)	4.4(1)	36(2)
2	232(15)	225(5)	240(15)	284(5)	36.4(10)	446(5)	54.6(10)	310(5)	39.3(10)	3.8(1)	30(2)	3.4(1)	33(2)
3	370(15)	345(5)	398(15)	415(5)	54.0(10)	671(5)	85.0(10)	457(5)	59.0(10)	3.2(1)	25(2)	2.9(1)	26(2)

TABLE I: Parameters characterizing the three exploited trap settings. The table shows the effectice atom-dimer temperature $T_{\rm eff}$, the temperature of the K atoms, $T_{\rm K}$, and the average dimer temperature, $\bar{T}_{\rm D}$. From the radial (axial) trap frequencies of K and Li, $\nu_{r(a),{\rm K}}$ and $\nu_{r(a),{\rm Li}}$, we determine the trap frequencies $\nu_{r(a),{\rm D}}$ of the dimers. We also show the axial and radial in-situ Gaussian widths of dimers (K atoms), $\sigma_{a,{\rm D(K)}}$ and $\sigma_{r,{\rm D(K)}}$, respectively.

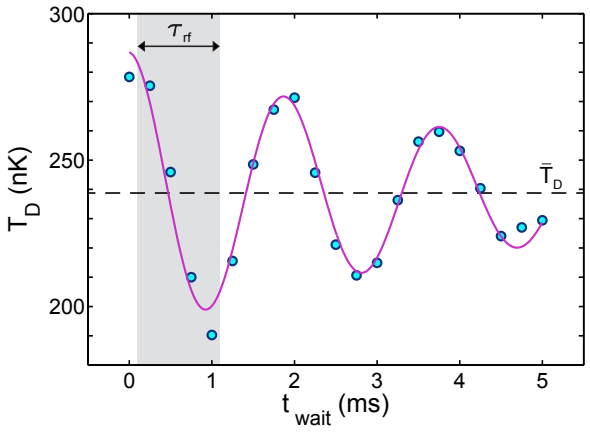

FIG. 3: Radial oscillation of the dimer cloud after the magnetic field ramp and the removal of the Li atoms. We plot the dimer temperature $T_{\rm D}$ versus the wait time $t_{\rm wait}$ after the first rf cleaning pulse to release from the trap. The filled circles are the experimental data, the solid line is a fit of a damped harmonic oscillation to the data. The shaded area indicates the time at which the spectroscopy rf pulses are applied and the dashed line marks the experimentally relevant averaged dimer temperature $\bar{T}_D$.

width $\sigma_{{\rm tof,K(D)}}$ the atom (dimer) temperature $T_{\rm K(D)}$ is given by

$$k_{\rm B}T_{\rm K(D)} = m_{\rm K(D)}\left(\sigma_{\rm tof,K(D)}/t_{\rm tof}\right)^2, \qquad (2)$$

where $m_{\rm K(D)}$ is the mass of the atom (dimer).

The magnetic field ramps and the removal of the surrounding Li shell, described in the previous section, excite collective oscillations of the dimer cloud. We trace these oscillations in momentum space as a function of a wait time $t_{\rm wait}$ after the cleaning procedure to release from the trap. An example of such an oscillation is shown in Fig. 3. In order to characterize the temperature at the time of the experiment, i.e. during the application of the 1-ms rf pulse (shaded area), we introduce the average temperature

$$\bar{T}_{\rm D} = \frac{1}{\tau_{\rm rf}}\int_{\rm rf} T_{\rm D}dt. \qquad (3)$$

Axial and radial sizes – To determine the densities of the atom (K) cloud and the dimer (D) cloud, we measure their Gaussian radial (r) and axial (a) widths $\sigma_{r,{\rm K(D)}}$ and $\sigma_{a,{\rm K(D)}}$, respectively. The axial widths are measured from a Gaussian fit to the axial profiles of in-situ absorption images. Since the radial widths are on the order of our imaging resolution, they can not be determined from in-situ images. We instead determine the radial widths of the K atom cloud as

$$\sigma_{r,{\rm K}} = \sqrt{\frac{k_{\rm B}T_{\rm K}}{m_{\rm K}(2\pi\nu_{r,{\rm K}})^2}}, \qquad (4)$$

where $T_{\rm K}$ and $\nu_{r,{\rm K}}$ denote the temperature and the radial trap frequency of the K atoms, respectively. Accordingly we determine the average radial in-situ width of the dimers,

$$\bar{\sigma}_{r,{\rm D}} = \sqrt{\frac{k_{\rm B}\bar{T}_{\rm D}}{m_{\rm D}(2\pi\nu_{r,{\rm D}})^2}}, \qquad (5)$$

using the averaged dimer temperature $\bar{T}_{\rm D}$, and the radial dimer trap frequency $\nu_{r,{\rm D}}$.

Trap frequencies of the dimers – We use the measured trap frequencies of the K and Li atoms to determine the trap frequencies $\nu_{r(a),{\rm D}}$of the LiK-dimers. Since the dimers are weakly bound over the magnetic field range investigated, their polarizabilities are approximately given by the sum of the polarizabilities of the Li and the K atoms. We want to point out that the differential light shift, shifting the FR center (see section A), gives only a $< 10\%$ correction to the trap potential and is neglected. Therefore, to a good aproximation, the dimer trap frequencies are given by

$$\nu_{a(r),{\rm D}} = \sqrt{(m_{\rm K}\nu^2_{a(r),{\rm K}} + m_{\rm Li}\nu^2_{a(r),{\rm Li}})/m_{\rm D}}, \qquad (6)$$

with $m_{\rm Li}$ being the mass of a Li atom.

Mean dimer density – For a given dimer number, $N_{\rm D}$, the mean dimer density experienced by the K atoms $\bar{n}_{\rm D}$ is given by

$$\bar{n}_{\rm D} = \frac{N_{\rm D}}{(2\pi)^{3/2}(\sigma^2_{r,{\rm K}} + \bar{\sigma}^2_{r,{\rm D}})\sqrt{\sigma^2_{a,{\rm K}} + \sigma^2_{a,{\rm D}}}}, \qquad (7)$$

where we have assumed Gaussian-shaped atom and dimer clouds.

Effective temperature – Due to heating and oscillations caused by our preparation procedure, the dimer temperature $T_{\rm D}$ in our system is different from the temperature of the non-interacting K$|2\rangle$ atoms that we use for rf spectroscopy. However, since our dimer and atom clouds are both non-degenerate, the energies of the atom-dimer collisions still assume a Boltzmann distribution. Averaging this distribution over the oscillations of the dimer cloud results in an effective atom-dimer collision temperature

$$T_{\rm eff} = \mu_3(T_{\rm K}/m_{\rm K} + \bar{T}_{\rm D}/m_{\rm D}), \tag{8}$$

where $\mu_3 = m_{\rm K}m_{\rm D}/(m_{\rm K}+m_{\rm D})$ is the atom-dimer reduced mass.

D. Importance of higher partial wave scattering and comparison to the equal-mass case

In this Section, we justify several important statements made in the main text. First, we have argued that the range of the atom-dimer interaction is comparable with the typical de Broglie wavelength and, therefore, quite a few partial waves are necessary to quantitatively characterize the line shift. In Fig. 4, we display $-\mathrm{Re}\, f(0)$, the quantity which is thermally averaged in the main text to obtain the line shifts. The method of calculating the scattering amplitude is described in Ref. [5]. Remarkably, the real part of the forward-scattering amplitude is seen to change sign at a collision energy much smaller than the binding energy, even for a relatively large detuning of 21 mG. The second change of sign of $-\mathrm{Re}\, f(0)$ seen in Fig. 4(a) is attributed to the fact that δ_p exceeds $\pi/2$ above $E_{\rm coll} \approx 0.1E_{\rm b}$, the point of the p-wave resonance. The p-wave contribution at larger collision energies then becomes positive (repulsive) [see Eq. (1) of the main text]. However, this peculiar phenomenon takes place only in a very close vicinity of the wide resonance limit as the p-wave phase shift drops rather abruptly with R^*/a [5]. We also note how, as the collision energy is increased, more and more partial wave channels are needed to accurately describe the forward-scattering amplitude. The calculation presented here includes the first 16 partial waves, which is sufficient to obtain an essentially converged scattering amplitude at the dimer breakup threshold.

As far as the equal mass case is concerned, the competition between the attraction in odd partial waves and repulsion in even partial waves is also quite significant, yet much less pronounced compared to the K-Li case. In Fig. 5 we display $-\mathrm{Re}\, f(0)$ as a function of $E_{\rm coll}$ for equal masses. Here the broad resonance case in Fig. 5(a) is relevant since it is readily available in current experiments and since there the effect of higher partial waves is most noticeable. We see that the forward-scattering amplitude does change sign in this case. However, in contrast to the K-Li case, this happens at a high collision energy close to the dimer breakup threshold and, in fact, already for $R^*/a \gtrsim 0.03$ the crossing is no longer on the scale. Thus, in the narrow resonance case illustrated in Fig. 5(b) and (c) the interaction is found to be repulsive below the dimer breakup threshold. In all cases the thermally averaged quantity $-\mathrm{Re}\,\langle f(0)\rangle$ is positive.

Finally, let us also make a remark concerning the thermal averaging of the scattering amplitude which we use in the main text. In principle, the averaging procedure requires the knowledge of the phase shifts above the atom-dimer breakup threshold. However, we always restrict ourselves to temperatures $k_{\rm B}T \lesssim E_{\rm b}/2$ and we check that in this case the integration result is insensitive to the exact extrapolation scheme. In practice we extrapolate the phase shift $\delta_l(k)$ using the log function, which works very well when we calculate the phase shifts above the breakup threshold in the Born-Oppenheimer approximation [6].

[1] D. Naik, A. Trenkwalder, C. Kohstall, F. Spiegelhalder, M. Zaccanti, G. Hendl, F. Schreck, R. Grimm, T. Hanna, and P. Julienne, Eur. Phys. J. D **65**, 55 (2011).

[2] C. Kohstall, M. Zaccanti, M. Jag, A. Trenkwalder, P. Massignan, G. M. Bruun, F. Schreck, and R. Grimm, Nature **485**, 615 (2012).

[3] C. Chin and P. S. Julienne, Phys. Rev. A **71**, 012713 (2005).

[4] F. M. Spiegelhalder, A. Trenkwalder, D. Naik, G. Kerner, E. Wille, G. Hendl, F. Schreck, and R. Grimm, Phys. Rev. A **81**, 043637 (2010).

[5] J. Levinsen, T. G. Tiecke, J. T. M. Walraven, and D. S. Petrov, Phys. Rev. Lett. **103**, 153202 (2009).

[6] J. Levinsen and D. Petrov, Eur. Phys. J. D **65**, 67 (2011).

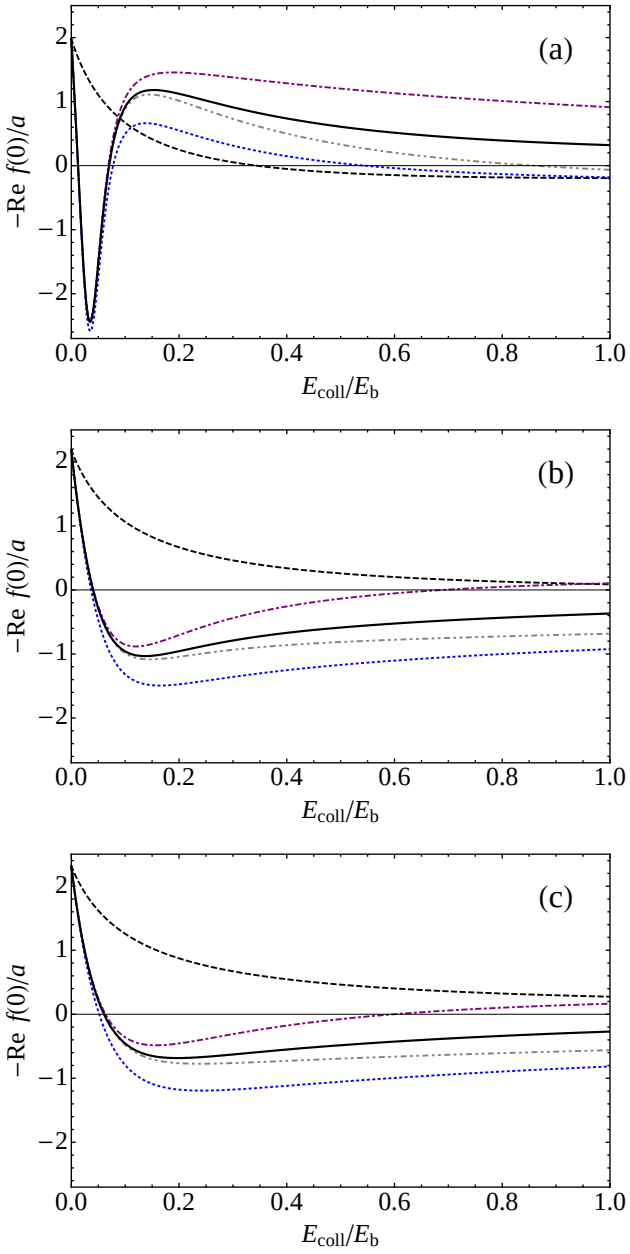

FIG. 4: Scattering of a ^{40}K atom with a ^{6}Li^{40}K dimer. The quantitiy $-\mathrm{Re}\, f(0)$ is plotted as a function of atom-dimer collision energy for (a) $R^*/a = 0$ [$B - B_0 = 0$], (b) $R^*/a = 1/2$ [$B - B_0 = -10\,\mathrm{mG}$], and (c) $R^*/a = 1$ [$B - B_0 = -21\,\mathrm{mG}$]. The lines are including s-wave scattering only (black, dashed), including up to p-wave (blue, dotted), up to d-wave (purple, dot-dashed), and up to f-wave (gray, double dot-dashed). The solid black line is $-\mathrm{Re}\, f(0)$ including the first 16 partial waves.

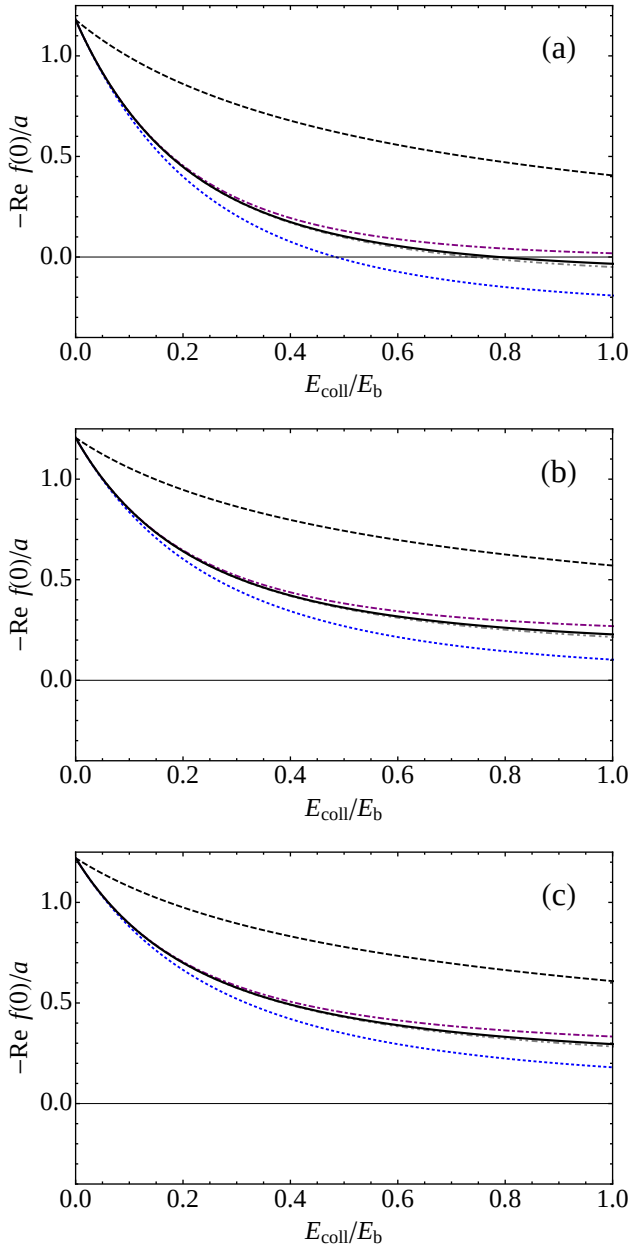

FIG. 5: Equal-mass case of atom-dimer scattering. We plot $-\mathrm{Re}\, f(0)$ as a function of collision energy for the homonuclear case, $m_\uparrow = m_\downarrow$. The conventions used for the lines as well as the detunings in (a) to (c) are the same as in Fig. 4. The solid black line includes the first 9 partial waves.